DOI: 10.1002/cite.201000064

Physical Adsorption Characterization of Nanoporous Materials

Matthias Thommes

During recent years, major progress has been made in the understanding of the adsorption, pore condensation and hysteresis behavior of fluids in novel ordered nanoporous materials with well defined pore structure. This has led to major advances in the structural characterization by physical adsorption, also because of the development and availability of advanced theoretical procedures based on statistical mechanics (e.g., density functional theory, molecular simulation) which allows to describe adsorption and phase behavior of fluids in pores on a molecular level. Very recent improvements allow even to take into account surface geometrical in-homogeneity of the pore walls However, there are still many open questions concerning the structural characterization of more complex porous systems. Important aspects of the major underlying mechanisms associated with the adsorption, pore condensation and hysteresis behavior of fluids in micro-mesoporous materials are reviewed and their significance for advanced physical adsorption characterization is discussed.

Keywords: adsorption, nanoporous materials, pore condensation hysteresis

Received: March 22, 2010; *accepted:* April 13, 2010

1 Introduction

In recent years major progress has been made concerning the synthesis of highly ordered nanoporous materials (pore width range from 2 – 50 nm) with tailored pore size and structure, controlled surface functionality and their applications ([1 – 5] and references therein). Advances have also been made in the synthesis and structural characterization of micro-mesoporous materials such as mesoporous zeolites [6 – 9] and hierarchically organized pore structures with an appropriate balance of micropores, mesopores and macropores, the latter being required to ensure the transport of the fluids to and from the smaller pores at a satisfactory rate. Recently, the synthesis of a novel class of alumina/silica transition metal based materials has been reported, which have partially pores between 1 and 2 nm, i.e, these novel materials bridge between zeolites and M41S materials [12]. An important new emerging class of solid state materials are metal-organic framework materials (MOFs), which offer a wide range of potential applications (e.g., gas storage, separation, catalysis, drug delivery) [13 – 16].

A comprehensive characterization of these porous materials with regard to pore size, surface area, porosity and pore size distribution is required in order to select and optimize the performance of nanoporous and hierarchically structured materials in many industrial applications [17 – 20].

In particular during the last decade, significant progress has been achieved in materials characterization and practical utilization because of major improvements in the understanding of the underlying mechanisms of adsorption in highly ordered mesoporous materials with simple geometries of known pore size (e.g., M41S materials) and consequently, in elaborating the theoretical foundations of adsorption characterization [22 – 24]. This has lead to the development of microscopic approaches such as the nonlocal density functional theory (NLDFT) and methods based on molecular simulation (e.g., Grand Canonical Monte Carlo simulation) which allow to describe adsorption and phase behavior of fluids in pores on a molecular level [25 – 30]. It has been demonstrated that the application of these novel theoretical and molecular simulation based methods leads to: (i) a much more accurate pore size analysis

An important new emerging class of solid state materials are metal-organic framework materials.

Appropriate methods for pore size analysis based on NLDFT and molecular simulation are meanwhile commercially available.

The van-der Waals forces and always include the long-range London dispersion forces and the short-range intermolecular repulsion.

[31, 32, 23], and (ii) allows performing pore size analysis over the complete micro/mesopore size range [e.g., 9, 21, 22, 32]. Appropriate methods for pore size analysis based on NLDFT and molecular simulation are meanwhile commercially available for many important adsorptive/adsorbent systems. This includes hybrid methods that assume various pore geometries for the micro- and mesopore size range, as it can be found for materials with hierarchical pore structures. The application of the NLDFT for micro-and mesopore size analysis has also been featured in ISO (International standard organization, ISO) standards [33].

These advances have been accompanied by the progress made in the development of various experimental techniques, such as gas adsorption, X-ray diffraction (XRD), small angle x-ray and neutron scattering (SAXS and SANS), mercury porosimetry, electron microscopy (scanning and transmission), thermoporometry, NMR-methods, and others [34 – 46]. In order to explore details of the adsorption mechanism and phase behavior of fluids in more complex porous systems (e.g., micro-mesoporous zeolites, hierarchically structured porous materials), it is advantageous to combine various experimental methods (e.g., coupling adsorption experiments with SAXS and SANS, i.e, in-situ-scattering [37, 42, 44 – 46]. However, among all these methods, gas adsorption is still the most popular one because it allows assessing a wide range of pore sizes, covering essentially the completed micro-and mesopore range. Furthermore, gas adsorption techniques are convenient to use and are less cost-intensive than some of the other methods. In recent years, automated adsorption equipment has been installed in almost every organization concerned with the synthesis and characterization of nanoporous materials. The development of commercial adsorption equipment has been accompanied by the installation of user-friendly data reduction software; nevertheless it is crucial to understand the fundamental principles involved in the interpretation of the isotherm data in order to arrive at a meaningful surface area and pore size analysis. In this paper focus is on some selected, important aspects of surface area and pore size analysis in particular in light of the progress made in this area over the last decade or so.

2 Physical Adsorption in Nanopores

2.1 General Aspects

Physisorption (physical adsorption) occurs whenever a gas (the adsorptive) is brought into contact with the surface of a solid (the adsorbent). The matter in the adsorbed state is known as the adsorbate, as distinct from the adsorptive, which is the gas or vapor to be adsorbed. The forces involved in physisorption are the van-der Waals forces and always include the long-range London dispersion forces and the short-range intermolecular repulsion. These combined forces give rise to nonspecific molecular interactions. Specific interactions come into play when polar molecules are adsorbed on ionic or polar surfaces but, as long as there is no form of chemical bonding, the process is still regarded as physisorption. Physical adsorption processes in porous materials is governed by the interplay between the strength of fluid-wall and fluid-fluid interactions as well as the effects of confined pore space on the state and thermodynamic stability of fluids confined to narrow pores. This is reflected in the shape or type of the adsorption isotherm. Within this context the International Union of Pure and Applied Chemistry (IUPAC) has published a classification of six types of adsorption isotherms [17] and proposed to classify pores by their internal pore width. The pore width is defined as the diameter in case of a cylindrical pore and as the distance between opposite walls in case of a slit pore), i.e., Micropore: pore of internal width less than 2 nm; Mesopore: pore of internal width between 2 and 50 nm; Macropore: pore of internal width greater than 50 nm. The micropore range is subdivided into those smaller than about 0.7 nm (ultramicropores) and those in the range from 0.7 – 2 nm (supermicropores). The pore size is generally specified as the internal pore width (for slit-like pores) pore radius/diameter (for cylindrical and spherical pores). It is important to note that the internal or effective pore width differs from the distance between the centers of surface atoms, which is usually employed in simulation work (i.e., the outer atoms of solid in the opposite walls of a pore). It has become popular to refer to micropores and mesopores as nanopores. The gas adsorption technique allows of course only to determine the volume of open pores. Closed porosity cannot be accessed, but can be derived if the true density and particle(bulk) density of the materials are known. Porosity is defined as the ratio of the volume of pores and voids to the volume occupied by the solid. Further, it should be noted that it is not always easy to distinguish between roughness and porosity. In principle, a simple convention is to refer to a solid as porous if the surface irregularities are deeper than they are wide.

The adsorbed amount as a function of pressure (or relative pressure P/P_0, where P_0 is the

saturation pressure of the adsorptive at a given temperature) can be measured by volumetric (manometric) and gravimetric methods, carrier gas and calorimetric techniques, nuclear resonance as well as by a combination of calorimetric and impedance spectroscopic measurements [34–47]. However, the most frequently used methods are the volumetric (manometric) and the gravimetric methods. The gravimetric method is convenient to use for the study of vapor adsorption not too far from room temperature, whereas the volumetric (manometric) method has advantages for the measurement of nitrogen, argon and krypton adsorption at cryogenic temperatures (77.4 K and 87.3 K), which are mainly used for surface area and pore size characterization [17]. Details concerning manometric (volumetric) and gravimetric experimental adsorption techniques can be found in [18–20, 48–52].

Nitrogen at 77 K is considered to be a standard adsorptive for surface area and pore size analysis, but it is meanwhile generally accepted that nitrogen adsorption is not satisfactory with regard to a quantitative assessment of the microporosity, especially in the range of ultramicropores (pore widths < 0.7 nm). Consequently, alternative probe molecules have been suggested, e.g., argon and carbon dioxide. For many microporous systems (in particular zeolites) the use of argon as adsorptive at its boiling temperature (87.3 K) appears to be very useful [9, 20–22, 24, 54]. When compared to nitrogen and carbon dioxide, it exhibits weaker attractive fluid-pore wall attractions for most adsorbents, which – during adsorption – does not give rise to specific interactions (like nitrogen and carbon dioxide because of their quadrupole moments) with most of surface functional groups and exposed ions. As a consequence, for instance in case of zeolites, argon fills micropores of dimensions 0.5–1 nm at much higher relative pressures (i.e., $10^{-5} < P/P_0 < 10^{-3}$) than nitrogen (i.e., $10^{-7} < P/P_0 < 10^{-5}$), which leads to accelerated diffusion and equilibration processes, and allows to obtain accurate high resolution adsorption isotherms within a reasonable time frame [19–21, 50]. Because of the lack of specific interaction between argon and the pore walls, the correlation between pore size and pore filling pressure is much more straightforward for argon as compared to nitrogen carbon dioxid. However, it has to be noted that contrary to 87.3 K, argon adsorption at liquid nitrogen temperature (77.4 K) is not the best choice for pore size/porosity characterization because of various reasons asscociated with the fact that at 77.4 K argon is ca. 6.5 K below the triple point temperature of bulk argon [22, 23, 20].

Despite the advantages which argon adsorption at 87.3 K offers, pore filling of ultramicropores still occurs at very low pressures (i.e,. turbomolecular pump vacuum is needed). Associated with the low pressures is as indicated above, the well-known problem of restricted diffusion, which prevents nitrogen molecules and also argon molecules from entering the narrowest micropores, i.e., pores of widths < ca. 0.45 nm. Alternatives for the determination of the total pore volume are CO_2 adsorption at room temperature. While CO_2 adsoption at 273 K is frequently used for the ultramicopore analysis of carbonaceous materials [53], it is not a good choice for the pore size analysis of materials with polar sites, mainly because of the very specific interactions that CO_2 can have with functional groups on the surface. However, it can still be used for assessing pore volume/porosity; the usefullness of CO_2 adsorption for the determining the pore volumes of NaX zeolites has been demonstrated (e.g, [54]).

Krypton adsorption at 77.4 K is more or less exclusively used for low surface area analysis of materials such as thin films [20] although some attempts to apply it for the pore size analysis of thin films have been reported as well [e.g., 55]. If applied at 87.3 K, Krypton adsorption also allows to obtain the pore size distribution of thin mesoporous silica films with pore diameters ranging from below 1 nm up to ~9 nm; although krypton at 87.3 K is ca. 30 K below the bulk triple point temperature, if confined to cylindrical silica pores with diameter < 9 nm it appears to be in a supercooled liquid state [56].

The gravimetric method is convenient to use for the study of vapor adsorption not too far from room temperature.

Restricted diffusion prevents nitrogen molecules from entering the narrowest micropores.

2.2 Adsorption Mechanism

The sorption behavior in micropores (pore width < 2 nm) is dominated almost entirely by the interactions between fluid molecules and the pore walls; in fact the adsorption potentials of the opposite pore walls are overlapping. As a consequence micropores fill through a continuous process (i.e., no phase transition). The filling of the narrowest micropores (i.e., of width equivalent to no more than two or three molecular diameters) takes place at low relative pressures (at $P/P_0 < 0.01$). This process has been termed "primary micropore filling" Filling of the wider micropores may occur over a much wider range of relative pressure ($P/P_0 \approx 0.01–0.2$). The enhancement of the adsorbent-adsorbate interaction energy in the pore center is now very small and the increased adsorption is mainly due to cooperative adsorbate-adsorbate interactions.

Micropores fill through a continuous process.

Hysteresis introdcues a considerable complication for pore size analysis.

In contrast, the sorption behavior in mesopores depends not only on the fluid-wall attraction, but also on the attractive interactions between the fluid molecules. This leads to the occurrence of multilayer adsorption and capillary (pore) condensation (at $P/P_0 > \approx 0.2$) the pore walls are covered by a multilayer adsorbed film at the onset of pore condensation. The stability of the adsorbed multilayer film for instance in a cylindrical pore is determined by the long-range van der Waals interactions, and by the surface tension and curvature of the liquid-vapor interface [23, 58–60]. For small film thickness the adsorption potential dominates. However, when the adsorbed film becomes thicker, the adsorption potential becomes less important, whereas surface tension/curvature effects become significant. At a certain critical thickness t_c, the multilayer film cannot be stabilized anymore, and pore condensation occurs in the core of the pore, controlled by intermolecular forces in the core fluid. Pore condensation represents a phenomenon whereby gas condenses to a liquid-like phase in pores at a pressure less than the saturation pressure P_0 of the bulk fluid. It represents an example of a shifted bulk transition under the influence of the attractive fluid-wall interactions. For pores of uniform shape and width (ideal slit-like or cylindrical mesopores) pore condensation can be classically described on the basis of the Kelvin equation [61], i.e., the shift of the gas-liquid phase transition of a confined fluid from bulk coexistence, is expressed in macroscopic quantities like the surface tension γ of the bulk fluid, the densities of the coexistent liquid ρ^l and gas ρ^g ($\Delta\rho = \rho^l - \rho^g$) and the contact angle θ of the liquid meniscus against the pore wall. For cylindrical pores the modified Kelvin equation [62] is given by: $\ln(P/P_0)\ -2\gamma\cos\theta/RT\Delta\rho(r_p - t_c)$, where R is the universal gas constant, r_p the pore radius and t_c the thickness of an adsorbed multilayer film, which is formed prior to pore condensation. The occurrence of pore condensation is expected as long as the contact angle is below 90°. A contact angle of 0° (i.e., complete wetting) is usually assumed in case of nitrogen and argon adsorption at 77.4 K and 87.3 K, respectively.

Adsorption hysteresis is considered as an intrinsic property of the vapor-liquid phase transition in a finite volume system.

The Kelvin equation provides a relationship between the pore diameter and the pore condensation pressure, and predicts that pore condensation shifts to a higher relative pressure with increasing pore diameter and temperature. Hence, the modified Kelvin equation serves as the basis for many methods applied for mesopore analysis, including the widely used Barett-Joyner-Halenda method (BJH). However, the validity of macroscopic, thermodynamic concepts such as the Kelvin equation and related methods becomes questionable for narrow mesopores (i.e, pore diameter smaller than ca. 15 nm (a comprehensive review is given in [23])

Capillary condensation is very often accompanied by hysteresis (Fig. 1), which of course introdcues a considerable complication for pore size analysis, but if interpreted correctly, provides important information about the pore structure/network, which is crucial for obtaining a comprehensive and accurate textural analysis of advanced nanoporous materials. Hysteresis can be observed in single pores as well as in pore networks [23, 67–71]. Generally, hysteresis is being considered: (i) on the level of a single pore of a given shape, (ii) cooperative effects due to the specifics of connectivity of the pore network, and (iii) in highly disordered, and for inhomogenous porous materials a combination of kinetic and thermodynamic effects spanning the complete disordered pore system has to be taken into account. Progress has been achieved in understanding the underlying internal dynamics of hysteresis in disordered pore systems [71], however a discussion of this topic is beyond the scope of this Section.

An empirical classification of hysteresis loops was given by IUPAC (Fig. 1), in which the shape of the hysteresis loops (types H1–H4) are correlated with the texture of the adsorbent. According to this classification, type H1 is often associated with porous materials exhibiting a narrow distribution of relatively uniform (cylindrical-like) pores. Materials that give rise to H2 hysteresis contain a more complex pore structure in which network effects (e.g., pore blocking/percolation) are important.

Isotherms with type H3 hysteresis do not exhibit any limiting adsorption at high P/P_0. This behavior can for instance be caused by the existence of non-rigid aggregates of plate-like particles or assemblages of slit-shaped pores and in principle should not be expected to provide a reliable assessment of either the pore size distribution or the total pore volume. H4 hysteresis loops are generally observed with complex materials containing both micropores and mesopores. Both, types H3 and H4 hysteresis contain a characteristic *step-down* in the desorption branch associated with the hysteresis loop closure.

On the pore level or independent pore model, adsorption hysteresis is considered as an intrinsic property of the vapor-liquid phase transition in a finite volume system. A classical scenario of capillary condensation implies that the vapor-liquid transition is delayed due to the existence of metastable adsorption films and

hindered nucleation of liquid bridges [67 – 70]. In open uniform cylindrical pores of finite length, these metastabilities occur only on the adsorption branch. Indeed, in an open pore filled by liquid-like condensate, the liquid-vapor interface is already present, and evaporation occurs without nucleation, via a receding meniscus. That is (as indicated before), the desorption process is associated with the equilibrium vapor-liquid transition, whereas hysteresis is caused by the fact that condensation occurs delayed due to the metastabilities associated with the nucleation of liquid bridges. Typically, a hysteresis loop of type H1 is observed. Meanwhile, modern, microscopic approaches such as non-local density functional theory (NLDFT) and molecular simulation (e.g, Grand Canonical Monte-Carlo simulation) are capable of qualitatively and quantitatively predicting the pore condensation and hysteresis behavior of fluids in ordered mesoporous materials . NLDFT correctly predicts (i) the positions of equilibrium vapor-liquid transition which is associated with the desorption branch of the isotherm in a pore of given size and geometry; (ii) the pressure where capillary condensation occurs by taking into account delayed condensation due to the metastability associated with the nucleation of liquid bridges (the resulting NLDFT method/kernel is based on so-called metastable adsorption isotherms) [31]. Hence, if the hysteresis is caused solely by the delayed condensation effect, the pore sizes calculated from the adsorption branch (by applying the NLDFT kernel of metastable adsorption isotherms) and desorption branch (by applying the NLDFT kernel of equilibrium isotherms) should be in agreement. This was indeed found for MCM-41, SBA 15 silicas [31, 23], which clearly confirmed the applicability of the so-called single (or independent) pore model for these materials. An example is shown in Fig. 2 which shows nitrogen adsorption in SB 15 silica.

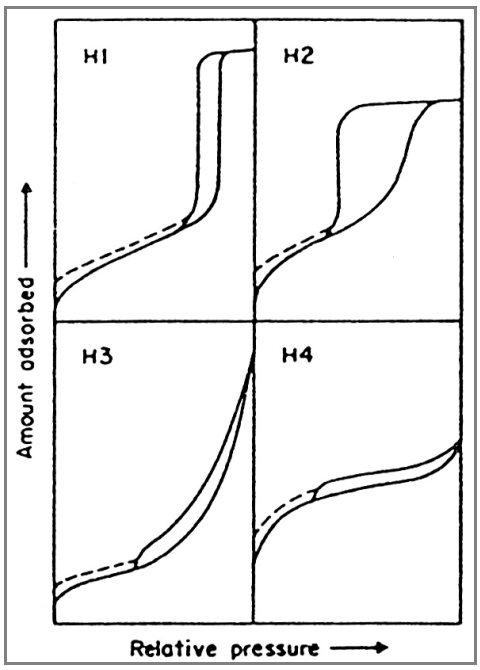

Figure 1. IUPAC classification of hysteresis loops.

Hysteresis in pore networks is expected to be more complex and very often hysteresis loops which reflect the shapes of types H2 to H4 are observed. However, some novel mesoporous materials such as MCM 48 and KIT 6 silica, which consist of ordered 3D pore networks can reveal perfect type H1 adsorption hysteresis [69 – 74], which indicates that pore channels do not exhibit constrictions which would otherwise give rise to type H2 hysteresis due to pore blocking/percolation effects and therefore would lead to deviations from type H1 hysteresis. However, it has been observed that hysteresis loops associated with the pore condensation of fluids (e.g., nitrogen, argon) in ordered three dimensional pore systems of

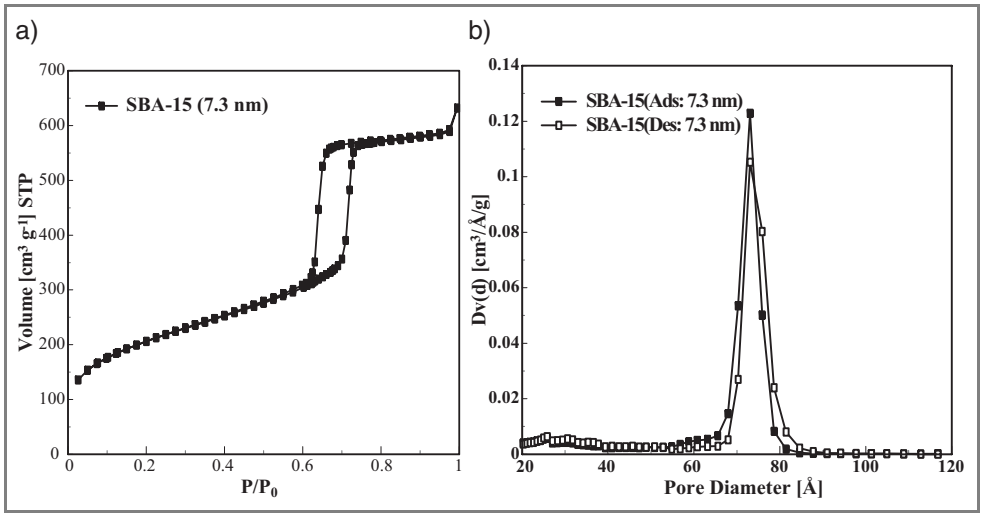

Figure 2. a) Nitrogen adsorption/desorption at 77.35 K in SBA-15silica.
b) NLDFT pore size distributions from adsorption- (application of NLDFT metastable adsorption isotherm kernel) and desorption (application of NLDFT equilibrium isotherms kernel).

Evaporation of the capillary condensate from a network of ink-bottle is obstructed by the pore constrictions.

It appears that that the interconnectivity of pores may lead to so-called the initiated/facilitated condensation.

MCM-48 or KIT-6 silica are generally more narrow as compared to the hysteresis loops observed in the pseudo-one-dimensional pore systems of MCM-41 or certain SBA-15 silica material [69, 71, 72]. This suggests that even in the absence of typical network effects (e.g., pore blocking) pore connectivity can have an impact on the width of the hysteresis loop, i.e,. it appears that that the interconnectivity of pores may lead to so-called the initiated/facilitated condensation [75, 78, 79, 80]. In pore networks neighbouring pores with a slightly smaller pore diameter are already filled with condensate, which exhibits a meniscus, and this interface can principally advance into larger neighbouring pores. This could then reduce the nucleation barriers associated with capillary condensation (in these slightly larger neighbouring pore segments) and therefore the pressure range over which metastable states extend. On the other hand, it is not to be expected (in the absence of pore blocking effects) that the interconnectivity of pores could have any appreciable influence on the position of the capillary evaporation. Hence, one should be able to calculate a reliable pore size distribution for ordered 3D systems from the desorption branch.

Hysteresis phenomena in pore networks consisting of ink-bottle type are quite complex. Two basic mechanisms of desorption in pore networks are distinquished as pore blocking percolation and cavitation. The former mechanism was introduced in the early studies of capillary hysteresis and, therefore is sometimes called *ink-bottle* or *classical pore blocking* mechanism [77–82]. It is well understood that evaporation the capillary condensate from a network of ink-bottle is obstructed by the pore constrictions. In this case, desorption from the pore body may occur only after emptying of its neck. In other words, desorption from the neck triggers evaporation in the blocked pore. Thus, the vapor pressure of desorption from the pore body depends on the neck size and network connectivity, as well as, on the state of the neighbouring pores. The onset of evaporation from the pore network is associated with the percolation treshhold and the formation of a continuous cluster of pores open to the external surface [80–86]. The percolation mechanism is observed in the pore networks with sufficiently large necks. Some typical pore structures where pore blocking is expected are shown in Fig. 3.

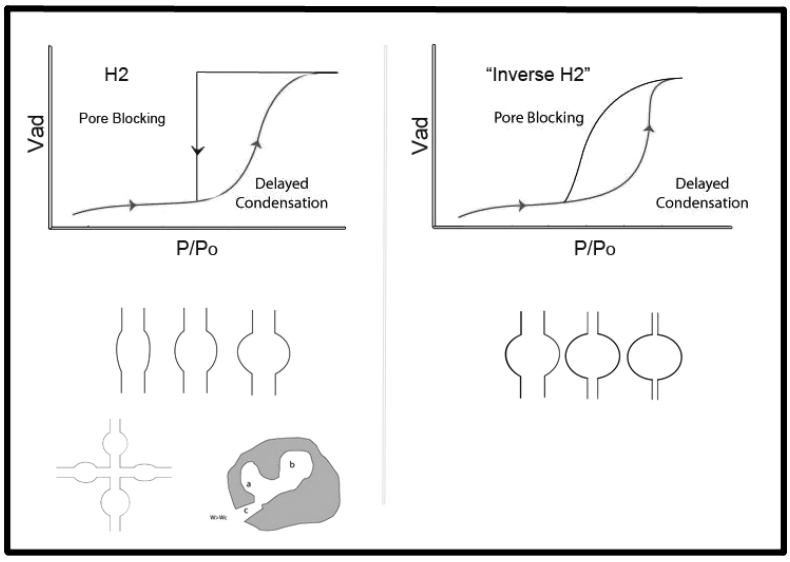

Figure 3. Schematic illustration of hysteresis in ink-bottle pores.

Conventional type H2 hysteresis will also occur in the case of a wide distribution of independent pores with the same or similar neck size, or in a network where the necksize distribution is much more narrow than the size distribution of the main cavities (e.g., pore blocking/percolation phenomena play and important role in porous vycor glass [35]). Recently, a different type of hysteresis loop, which looks somewhat like an inverse type H2 hysteresis has been associated with the occurrence of pore blocking as well (Fig. 3). In this case the desorption branch is less steep than the adsorption branch. Such hysteresis could be observed in materials where the pore size distribution of the main pores is more narrow than the pore size distribution of the entrance(neck) diameters. Inverse type H2 hysteresis has been observed for instance in mesoporous foam consisting of polyhedral foam cells of 60–70 nm diameter, interconnected by cylindrical access channels with several characteristic sizes for the latter [47], or in materials such as FDU-1 silica [91] or KIT-5 silica [92], where the entrances to the spherical pores had been widened by either calcination and or hydrothermal treatment, respectively. In this case, the distribution of necks/constrictions is much wider than the distribution of main pore cavities, therefore the adsorption/condensation branch is much steeper than the desorption branch. Hence, the distribution of neck sizes can be obtained from an analysis of the desorption branch, whereas the pore/cavity size distribution is only available from an analysis of the adsorption branch (e.g., by applying a method for pore size analysis which correctly takes into account the delay in condensation such as the NLDFT kernel of metastable adsorption isotherms; Fig. 2) .

Theoretical and experimental studies [32, 94] have revealed that if the neck diameter is smaller than a certain critical width (estimated to be ca. 6 nm for nitrogen at 77.4 K), the me-

chanism of desorption from the pore body involves cavitation - spontaneous nucleation and growth of gas bubbles in the metastable condensed fluid (Fig. 4). In this case, the pore body empties while the pore neck remains filled. It is important to note that if the pore neck is below the critical neck size, the actual width of the pore neck appears not to play any role for the pressure where cavitation occurs, i.e., the cavitation pressure depends essentially on the thermophysical properties of the fluid in the main pore cavity. Cavitation controlled evaporation can for instance be found in materials such as SBA-16 [e.g., 99] and in silicas with hierarchical pores structures such as KLE, and KLE/IL silica [32], mesoporous zeolites [e.g., 9] and some clays [e.g., 100]. As mentioned before, it is expected that at a given temperature, the neck size controls whether pore blocking or cavitation occurs. Above a certain critical neck size (≈ 6 nm) pore blocking occurs, and below this cavitation controlled evaporation takes place. Hence, by varying the neck size/entrances to the main pore system, one should be able to observe such a transition from cavitation induced evaporation to pore blocking. Indeed such results have been reported for SBA-16 silica [99], FDU-1 silica [91], and KIT-5 silica [92]. On the other hand, the same phenomena can be observed by varying the temperature of the adsorption experiment for a given adsorbend with ink-bottle geometry.

In order to detect which mechanism is dominant, an adsorption test was suggested in [32]. This test is based on measuring adsorption isotherms with different adsorbates (such as nitrogen and argon) and/or at different temperature and comparing PSDs calculated from the data obtained at these different conditions. In the case of pore blocking, the pressure of evaporation is controlled by the size of connecting pores. Therefore, PSDs calculated from the desorption branches should be independent of the choice of the adsorbate or temperature. This has indeed been found for instance in porous vycor glass which is known to give rise to pore blocking/percolation phenomena [32]. In the case of cavitation, the pressure of desorption depends on the adsorbate and temperature and is not correlated with the size of connecting pores. Hence, PSDs calculated from the desorption branch of the hysteresis loop are artificial; they do not reflect the real pore sizes and they should depend on the choice of the adsorptive and/or temperature which had been demonstrated for various silica materials with hierarchical pore structures [32, 101].

In addition to hierarchically structured materials (e.g. KLE/IL silica), and micro-mesoporous zeolites, plugged hexagonal templated silica (PHTS) material with combined micro- and mesopores and a tunable amount of both open and inkbottle pores gained recently some attention [102, 103] Fig. 5 shows a schematic isotherm typical for adorption in plugged SBA-15 silica.

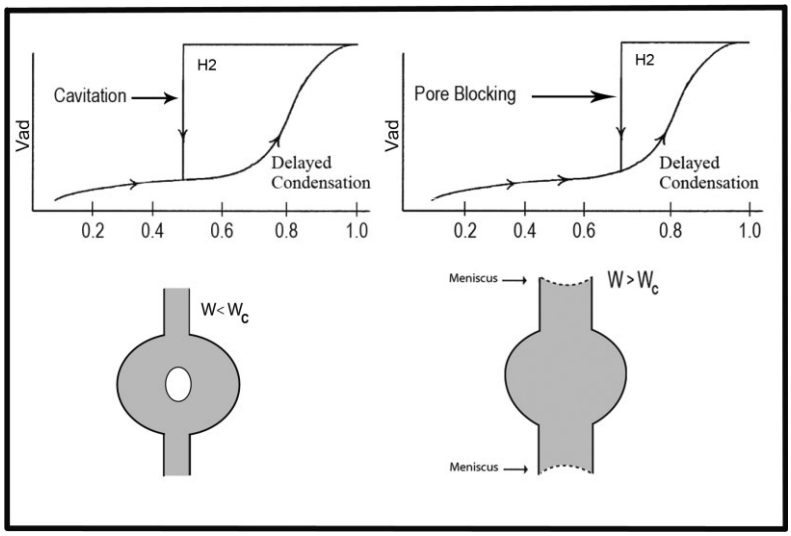

Figure 4. Schematic illustration of pore blocking and cavitation controlled evaporation. Adapted from [32].

At a given temperature, the neck size controls whether pore blocking or cavitation occurs.

The adsorption/desorption isotherm is consistent with a structure which exists of both open and blocked cylindrical mesopores. The two-sep desorption isotherm indicates the occurrence of both equilibrum evaporation/desorption and pore blocking/cavitation effects. The desorption at higher pressures is associated with the evaporation of liquid from open pores. On the other hand, blocked mesopores remain filled until they empty via cavitation.

Based on the discussed examples, it appears that cavitation induced evaporation appears to be important for many micro/mesoporous solids and is responsible for the often observed characteristic step down in the desorption isotherms associated with hysteresis loop closure (see type H3 and H4 hysteresis loops in the IUPAC classification (Fig. 1). In the past, this characteristic step down was discussed within the framework of the clasccial tensile strength hypothesis [18, 104 – 106]. Here it was assumed

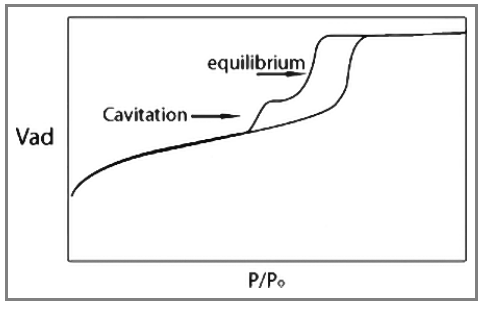

Figure 5. Characteristic sorption isotherm as it can be found in plugged cylindrical pores.

The onset of cavitation depends on pore/cavity size and pore geometry for for pore diameters smaller than ≈ 11 nm, but remains practically unchanged for samples with large pores.

that the tensile stress limit of condensed fluid (the pressure where cavitation induced evaporation occurs) does not depend on the nature and pore structure of the adsorbent, yet is a universal feature of the adsorptive. However, in contrast to this classical viewpoint, very recent work has clearly revealed that the onset of cavitation (and the so-called lower closure point of hysteresis) depends on pore/cavity size and pore geometry for for pore diameters smaller than ≈ 11 nm, but remains practically unchanged for samples with large pores [101].

3 Surface Area and Pore Size Analysis

3.1 Application of the BET (Brunauer, Emmett and Teller) method

Surface area is a crucial parameter for optimizing the use of porous materials in many applications.

Surface area is a crucial parameter for optimizing the use of porous materials in many applications, and has also recently be discussed in context with the novel class of Metal-Organic-Framework (MOF) materials, where extremely high specific surface areas (> 3000 m^2g^{-1}) have been reported [e.g., 14]. Due to the complex nature of micro/mesoporous materials no single experimental technique can be expected to provide an evaluation of the *absolute* surface area, however the most frequently applied method is the BET method introcuded more than sixty years ago by Brunauer, Emmett and Teller [103]. Usually, two stages are involved in the evaluation of the BET area. First, it is necessary to transform a physisorption isotherm into the 'BET plot' and from there to derive the value of the BET monolayer capacity, n_m. The second stage is the calculation of the specific surface area, S, which requires knowledge of the molecular cross-sectional area. The monolayer capacity n_m is calculated from the adsorption isotherm using the BET equation (Eq. (1))

Nitrogen is usually considered the standard adsorptive, also because of the availability of liquid nitrogen.

$$1/[n((P_0/P)\text{-}1)] = (1/n_mC) + [(C\text{-}1)/n_mC]\ (P/P_0) \quad (1)$$

where n is the adsorbed amount, n_m is the monolayer capacity and C is an empirical constant which gives an indication of the order of magnitude of the attractive adsorbent-adsorbate interactions. In the original work of Brunauer, Emmett and Tellerit was found that type II nitrogen isotherms (according to the IUPAC classification [10]) on various nonporous adsorbents gave linear BET plots over the approximate range $p/p^\circ - 0.05 - 0.3$. The specific surface area S can then be obtained from the monolayer capacity n_m by the application of the simple equation: $S = N_m L\sigma$, where L is the Avogadro constant and σ is the so-called cross-sectional area (the average area occupied by each molecule in a completed monolayer).

The BET equation is applicable for surface area analysis of nonporous- and mesoporous materials consisting of pores of wide pore diameter, but is in a strict sense not applicable for microporous adsorbents (for a critical appraisal of the BET method is given in [19, 20]). Hence, the surface area obtained by applying the BET method on adsorption isotherms from microporous materials reflects as a kind of apparent or equivalent BET area [19]. A problem directly related to the discussion concerning the applicability of the BET method for assessing the surface areas of microporous materials is the determination of the proper relative pressure range for applying the BET method. If the BET equation is applied within it's classical range (rel. pressure range 0.05 – 0.3) on adsorption data obtained on microporous materials, one does very often not find a linear range, the C-constant maybe negative (which is unphysical) and the obtained BET area depends on the selected data points. Recently a procedure was suggested which allows to determine this *linear BET range* for microporous materials in an unambiguous way [101]. This approach has been applied for zeolites [22], metal-organic framework materials [105] as well is recommended in a very recent standard of the International Standard Organization (ISO) [106].

Also with regard to the determination of surface areas via the BET method it is of interest discuss the choice of the adsorptive. Nitrogen is usually considered the standard adsorptive, also because of the availability of liquid nitrogen. A key parameter for a proper BET analysis is the assumption of a cross-sectional area, i.e., the area occupied by an adsorbed molecule in a complete monolayer. It is known that the quadrupole moment of the nitrogen molecule leads for instance to specific interactions with polar hydroxyl surface groups, causing an orientating effect on the adsorbed nitrogen molecules [106]. Consequently, on polar surfaces the effective cross-sectional area of adsorbed nitrogen is smaller than the customary value of 0.162 nm^2. Indeed, recent experimental sorption studies on highly ordered mesoporous silica materials such as MCM-41 suggest strongly that the cross-sectional area of nitrogen on a hydroxylated surface might differ from the commonly adopted value of 0.162 nm^2 [111, 112]. Based on measurements of the nitrogen volume adsorbed on silica spheres of known diameter.

In [108] a cross-sectional area of 0.135 nm^2 was proposed. Consequently, using the standard cross-sectional area (0.162 nm^2) the BET surface area of hydroxylated silica or other po-

lar surfaces can be significantly overestimated. Hence, since argon molecule is monatomic and much less reactive than the diatomic nitrogen molecule, argon adsorption (at 87 K) is an alternative adsorptive for surface area determination. Due to the absence of a quadrupole moment and the higher boiling temperature, the cross-sectional area of argon (0.142 nm^2 at 87.3 K) is less sensitive to differences in the structure of the adsorbent surface [22].

3.2 Pore Size Analysis

In absence of mesoporosity, the physisorption isotherm is of type I with a plateau which is virtually horizontal. In this case the adsorbed amount in the plateau region can be directly correlated with the micropore volume by applying the so-called Gurvich rule [17 – 20]. Here it is assumed that the pores are filled with a liquid adsorptive of bulk-like properties, an assumption that does not allow for the fact that the degree of molecular packing in small pores is dependent on both pore size and pore shape. In case of additional mesoporosity, the micropore volume can be obtained by applying the standard and comparison isotherm concept (e.g. t-plot), or the Dubinin-Radushkevich approach [14 – 20, 114]; here it is also assumed that the micropores are filled by a homogeneous liquid phase with bulk-like properties. Other approaches such those of Horvath and Kawazoe (HK), Saito and Foley (SF) and Cheng-Yang (CY) [19, 20, 114, 115] allow to obtain the pore size distribution in addition to the pore volume, but rely on similar macroscopic, thermodynamic assumptions concerning the nature of confined adsorbate. This leads to inaccuracies in the pore volume and pore size determination. In case of mesoporosity, the total pore volume via Gurvich rule is determined from the adsorbed at relative pressure 0.95 in case of type isotherms with H1 and H2 hysteresis loops. Pore size analysis of mesoporous materials can be performed with methods based on the the macroscopic Kelvin equation, e.g., Barett-Joyner-Halenda (BJH approach) [19, 20, 66]). Direct experimental tests of the validity of the Kelvin equation were made possible by using for instance MCM-41 silica as a model material, which consists of an array of independent cylindrical pores (of the same diameter in the range 2 nm to 10 nm). Because of the high degree of order, the pore diameter can be derived by independent methods (based on X-ray-diffraction, high-resolution transmission electron microscopy etc.). It was found that the BJH method and related procedures based on a modified Kelvin equation can underestimate the pore size by up to 20 – 30 % for pores smaller than 10 nm (for a comprehensive review, please see [23] and references therein). This deviations are caused by a series of problems, including the fact that the assessment of pre-adsorpbed film thickness also becomes problematic when the pore diameter decreases [23, 20]. An improvement for pore size analysis can be obtained by calibrating the Kelvin equation using a series of MCM-silicas of known pore diameter (obtained from XRD interplanar spacing and the mesopore volume). In this manner, a relation between capillary condensation pressures and pore size can be established and used to obtain an empirically corrected Kelvin equation valid over the calibrated range (~ 2 – 10 nm) [118, 119].

Argon adsorption at 87 K is an alternative adsorptive for surface area determination.

It is further evident that the Kelvin concept fails to describe correctly the peculiarities of the critical region and the confinement-induced shifts of the phase diagram (i.e., critical point shifts, freezing point and triple point shifts, etc) of the pore fluid [23]. The thermodynamic state and the thermophysical properties of the adsorbed pore fluids, as already indicated, differ significantly from the bulk fluid, and this has a pronounced effect on the shape of the adsorption isotherm; e.g., the disappearance of hysteresis with decreasing pore size (at given temperature), or increasing temperature (for a given pore size) cannot be described by the Kelvin equation [23]. However, microscopic methods based on statistical mechanics which can describe the configuration of the adsorbed phase on a molecular level (DFT, molecular simulation) take this into account.

The Kelvin concept fails to describe correctly the peculiarities of the critical region and the confinement-induced shifts of the phase diagram.

It has been shown that the non-local density functional theory (NLDFT) with suitably chosen parameters of fluid-fluid and fluid-solid interactions quantitatively predicts the positions of capillary condensation and evaporation transitions of argon and nitrogen in cylindrical and spherical pores of ordered mesoporous molecular sieves (e.g., MCM-41, SBA-15, SBA-16, and hierarchically structured silica materials), [e.g., 31, 32, 120]. To practically apply this approach for the calculation of the pore size distributions from the experimental adsorption isotherms, theoretical model isotherms have to be calculated using methods of statistical mechanics. In essence, these isotherms are calculated by integration of the equilibrium density profiles of the fluid in the model pores. A set of isotherms calculated for a set of pore sizes in a given range for a given adsorbate is called a kernel, and can be regarded as a theoretical reference for a given adsorption system. Such a kernel can then be used to calculate pore size distributions from adsorption/desorption isotherms measured for the corresponding sys-

A DFT kernel can be regarded as a theoretical reference for a given adsorption system and can then be used to calculate pore size distributions from adsorption/desorption isotherms measured for the corresponding systems.

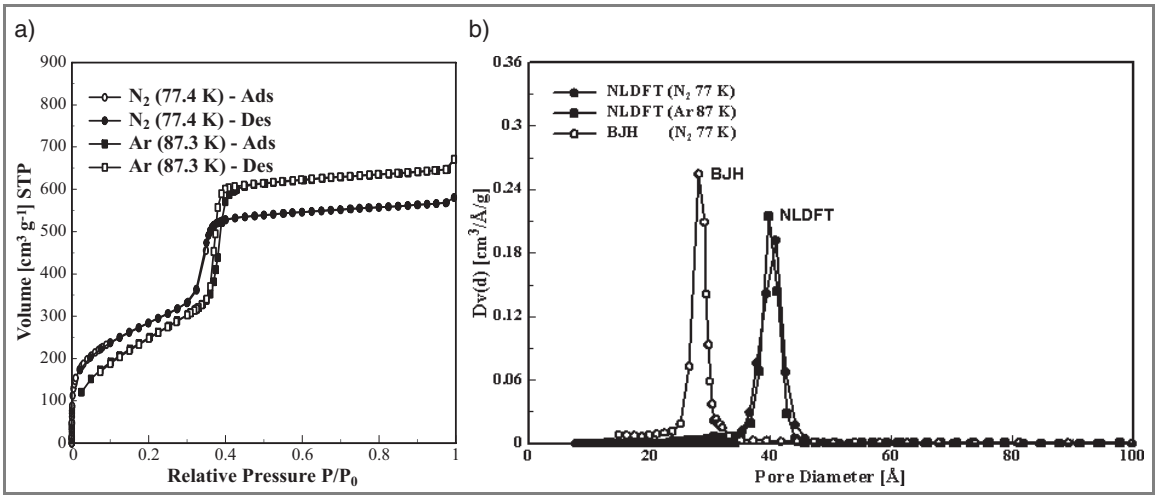

Figure 6. a) Nitrogen and argon sorption isotherms at 77 K, and 87.3 K, respectively in MCM-41 silica and NLDFT fit b) NLDFT (from argon and nitrogen isotherms) and BJH (from nitrogen isotherm) pore size distribution curves.

tems. It is important to realize that the numerical values of a given kernel depend on a number of factors, such as the assumed geometrical pore model, values of the gas-gas and gas-solid interaction parameters, and other model assumptions. The calculation of pore size distribution is based on a solution of the Integral Adsorption Equation (IAE), which correlates the kernel of theoretical adsorption/desorption isotherms with the experimental sorption isotherm (for details see [21, 23, 31]). Comparing the calculated NLDFT (fitting) isotherm with the experimental sorption isotherm allows to check the validity of the calculation. Pore size analysis data obtained in this way for mesoporous molecular sieves obtained with NLDFT methods agree very well with the results obtained from independent methods (e.g. based XRD, TEM etc.).

The application of the NLDFT for the pore size analysis of highly ordered MCM-41 materials is shown in Fig. 6. Fig. 6a shows nitrogen and argon isotherms at 77 K and 87 K, respectively. The nitrogen isotherm is fully reversible, whereas argon adsorption shows a small but genuine hysteresis loop, indicating the differences of thermodynamics between the confined argon and nitrogen states. However, the NLDFT pore size distribution curves calculated from the nitrogen and argon desorption isotherms by applying dedicated NLDFT methods assuming nitrogen (77.4 K) and argon (87.3 K) sorption in cylindrical silica pores agree perfectly. On the other hand, the BJH pore size distribution obtained from the reversible nitrogen isotherm underestimates significantly the pore size.

Methods based on DFT and molecular simulation allow to obtain an accurate pore size analysis over the complete micro/mesopore size range with a single method.

Another major advantage of methods based on DFT and molecular simulation is that they allow to obtain an accurate pore size analysis over the complete micro/mesopore size range with a single method as demonstrated in Fig. 7, which shows argon sorption at 87.3 K in a micro-mesoporous ZSM-5 zeolite and resulting pore size analysis. A type H4 hysteresis loop has been observed, with the characteristic step down at rel. pressures ≈ 0.4. The pore size distribution (psd) was obtained by applying a hybrid NLDFT method which assumes argon adsorption in a cylindrical, siliceous zeolite pore in the micropore range, and a amorphous (cylindrical) silica pore model for the mesopore range . Two different types of hybrid kernel for adsorption and desorption branches were applied. The adsorption branch kernel takes correctly into account the delay in condensation due to metastable pore fluid, whereas a equilibrium NLDFT kernel was applied to the desorption branch. The NLDFT pore size distribution clearly shows two distinct groups of pores: micropores of the same size as in ZSM-5 (0.52 nm) and primary mesopores in the pore diameter range from 2 – 4 nm.

The pore size distribution curves obtained from adsorption and desorption branches agree with exception of the PSD artifact obtained from the section of desorption branch with the characteristic step-down in the desorption isotherm. As discussed in Sect. 2.2, this step down is not associated with the evaporation of pore liquid from a specific group of pores, i.e., the spike in the desorption pore size distribution curve (PSD) reflects an artifact, caused by the spontaneous evaporation of metastable pore liquid (cavitation, i.e., the tensile strength effect). In contrast, the PSD derived from the adsorption branch does not reveal this artifical PSD peak.

While NLDFT has been demonstrated to be a reliable method for the characterization of a

variety of ordered and hierarchically structured materials, a drawback of the standard NLDFT is that they do not take sufficiently into account the chemical and geometrical heterogeneity of the pore walls (e.g., of carbon materials).Usually a structureless (i.e., chemically and geometrically smooth) pore wall model is assumed. The consequence of this mismatch between the theoretical assumption of a smooth and homogeneous surface and the experimental situation is that the theoretical DFT adsorption isotherms exhibit multiple steps associated with layering transitions related to the formation of a monolayer, second adsorbed layer, and so on. Experimentally, stepwise adsorption isotherms are observed only at low temperatures for fluids adsorbed onto molecularly smooth surfaces, such as mica or graphite. However, in amorphous porous materials layering transitions are hindered due to inherent energetic and geometrical heterogeneities of real surfaces. The layering steps on the theoretical isotherms can cause artificial gaps on the calculated pore size distributions, because the computational scheme, which fits the experimental isotherm as a linear combination of the theoretical isotherms in individual pores, attribute a layering step to a pore filling step in a pore of a certain size. The problem is enhanced in many porous carbon materials, which exhibit in contrast to micro-mesoporous zeolites broad PSD's, and here the artificial layering steps obtained in the theoretical isotherms cause artificial gaps on the calculated pore size distributions. This problem has been addressed by various approaches [121 – 124] including the so-called QSDFT (quenched solid density functional theory) [122, 123]. QSDFT allows to take into account wall heterogeneity in a straightforward way. It has been shown that QSDFT significantly improves the method of adsorption porosimetry for heterogenous porous carbons, the pore size distribution (PSD) functions do not possess anymore the artificial gaps in the regions of ~1 nm and ~2 nm [123]. This is demonstrated in Fig. 8 in which the pore size distribution calculations for active carbon fiber ACF-15 for the nitrogen adsorption isotherm are presented and the QSFDFT and NLDFT results are compared. Fig. 8a shows the fit of the experimental isotherm with the calculated theoretical one. The QSDFT provides a significant improvement in the agreement between the experimental and the theoretical isotherms, in particular in the low pressure range of the micropore filling (Fig. 8a). The prominent step at $P/P_0 \sim 3 \cdot 10^{-4}$ that is characteristic to the theoretical NLDFT isotherms, is due to the monolayer transition on the smooth graphite surface, is completely eliminated in the QSDFT isotherm. As a consequence, a sharp minimum in the NLDFT pore size distribution curve at ~1 nm, which is typical to the NLDFT pore size distribution curves for many microporous carbons, does not appear in QSDFT calculations (Fig. 8b). This confirms that this minimum on the differential NLDFT pore size distribution is indeed an artifact caused by the monolayer step in NLDFT approach, which occurs at the same pressure as the pore filling in a ~1 nm slit pore. The pore size distribution curves in Fig. 8b show that QSDFT and NLDFT agree beyond the regions where artificial gaps were observed with NLDFT. It clearly follows that the application of QSDFT leads to major improvements in the pore size analysis of nanoporous carbon materials.

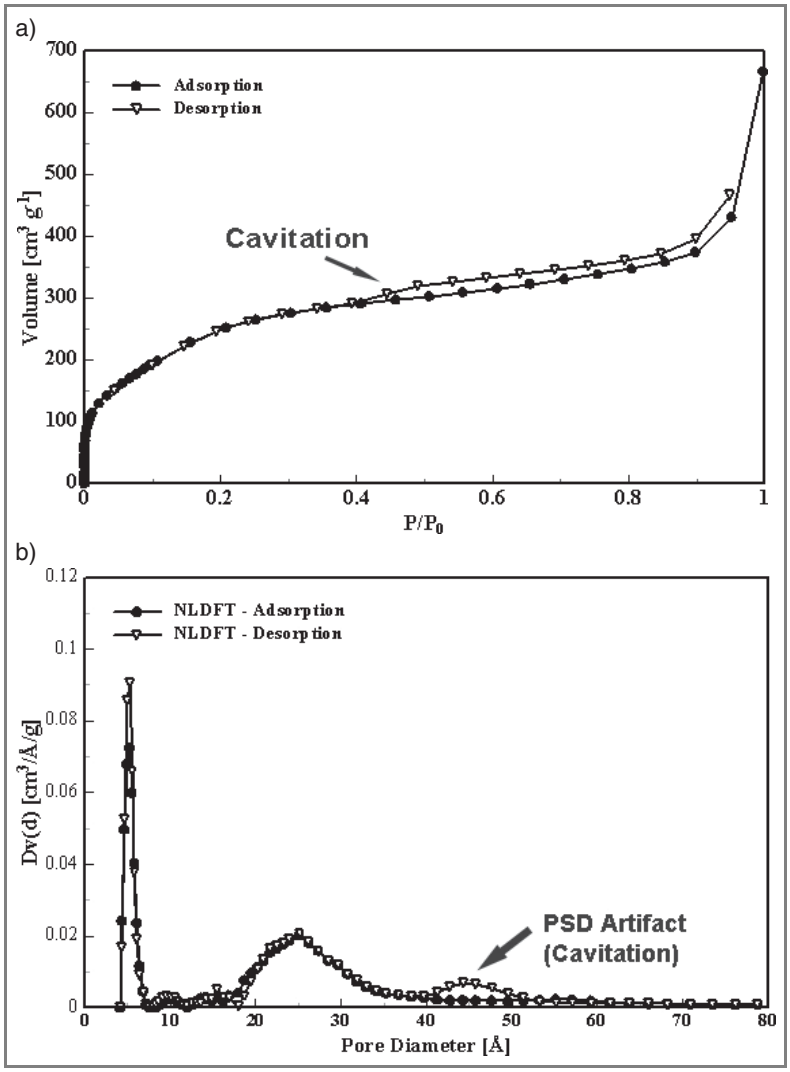

Figure 7. a) Nitrogen adsorption in micro-mesoporous ZSM5 zeolite. b) NLDFT pore size analysis by applying the NLDFT metastable adsorption branch kernel on the adsorption isotherm and the equilibrium transition kernel on the desorption data.

QSDFT significantly improves the method of adsorption porosimetry for heterogenous porous carbons.

However, it should be noted that the application of QSDFT and other of these advanced

methods is useful and leads to accurate results only, if the given experimental adsorptive/adsorbent system is compatible with the chosen NLDFT or GCMC kernel.

5 Summary and Conclusion

The major progress made in the understanding of the adsorption, pore condensation and hysteresis behavior of fluids in nanoporous materials has led to major advances in the structural characterization by physical adsorption, also because of the development and availability of advanced theoretical procedures based on statistical mechanics (e.g., Non-Local Density Functional Theory (NLDFT)) and molecular simulation. Contrary to classical, macroscopic thermodynamic approaches, these microscopic methods describe the configuration of the adsorbed phase on a molecular level. The validity of these advanced models (in particular NLDFT) for pore size analysis could be confirmed with the help of ordered mesoporous molecular sieves of known pore size and structure. It has been demonstrated that the application of these novel theoretical and molecular simulation based methods leads to: (i) a much more accurate pore size analysis, and (ii) allows performing pore size analysis over the complete micro/mesopore size range. NLDFT is meanwhile widely used for pore size analysis, featured in an ISO standard and commercially available. While NLDFT has been demonstrated to be a reliable method for characterization of ordered and hierarchically structured materials, a drawback of the standard NLDFT is that they do not take sufficiently into account the chemical and geometrical heterogeneity of the pore walls. These deficiencies are currently being addressed by various scientific groups; a novel DFT method, namely QSDFT (quenched solid density functional theory) accounts for the surface geometrical in-homogeneity in form of a roughness parameter. Application of QSDFT leads to major improvements in the pore size analysis of nanoporous carbon materials.

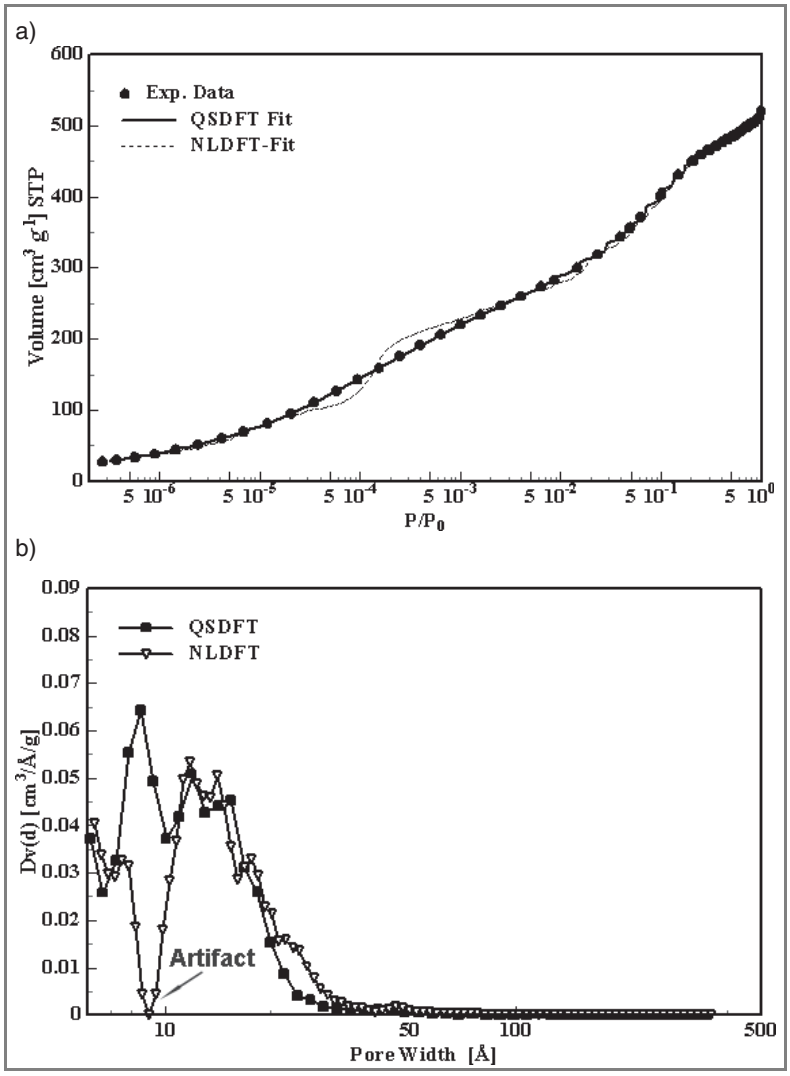

Figure 8. Comparison of the QSDFT and NLDFT methods for nitrogen adsorption for activated carbon fiber ACF-15.
a) Experimental isotherm (in semi-logarithmic scale) together with the NLDFT and QSDFT theoretical isotherms.
b) NLDFT and QSDFT differential pore size distributions.

More recently, the focus has shifted towards the structural analysis of advanced micro-mesoporous materials (e.g., micro-mesoporous zeolites, and hierarchically structured porous materials), which have many potential applications (e.g., in catalysis, separations, etc.). A combination of various phenomena including micropore filling, pore condensation, pore blocking/percolation and cavitation induced evaporation can be observed, which is reflected in characteristic types of adsorption hysteresis. These complex hysteresis loops introduce of course a considerable complication for pore size analysis, but if interpreted correctly, also allow to obtain important and unique information about the pore structure of such advanced micro-mesoporous material.

In addition to nitrogen adsorption at 77 K, it is suggested to use complimentary probe molecules (e.g., argon at 87 K) not only to check for consistency, but also to obtain more accurate and comprehensive surface area, pore size and pore structure information. Within this the importance of coupling gas adsorption with other experimental techniques (e.g. x-ray and neutron scattering based techniques) for studying details of the adsorption and phase behavior of fluids in complex pore networks needs to be pointed out.

Despite the progress made in theoretical and molecular simulation based approaches to develop more realistic adsorbent models, there are still major problems in the characterization

of disordered porous materials and mesoporous with imhomogeneous surface chemistry (incl. materials with chemically functionalized surfaces,). New challenges are also associated with just emerging new types of porous materials, such as metal-organic framework materials covalent organic frameworks (COFs), as well as materials with non-rigid pore structures. This needs to be addressed in future experimental and theoretical work with advanced theoretical, computational and experimental approaches, and well chosen model materials.

I would like to thank Maritza Roman for help with the graphics.

Dr. M. Thommes
(matthias.thommes@quantachrome.com),
Quantachrome Instruments
1900 Corporate Drive
Boynton Beach
Fl-33426, USA.

Matthias Thommes received his Doctorate in Physical Chemistry with Prof. G.H. Findenegg at Ruhr University Bochum (1989 – 1991) and Technical University Berlin (1992/93). From 1992 – 1995 Dr. Thommes was a Research Associate at the Iwan-N.-Stranski Institute of Physical and Theoretical Chemistry, Technical University Berlin and Project Scientist for a microgravity experiment on critical adsorption. From 1996 to 1997, he was an ESA fellow (European Space Agency) and Postdoctoral Research Associate at the University of Maryland at College Park, USA. Dr. Thommes is a member of the Board of Directors of the International Adsorption Society (IAS; since 2007), a Council Member of the International Mesotructured Materials Association (IMMA, 2006-2010), and a member of the Advisory Board of the journal *Part. Part. Syst. Char.*. He is the chairman of the IUPAC taskgroup on *Physisorption of Gases, with special reference to the evaluation of surface area and pore size distribution.*

References

[1] D. Zhao, Y. Wang, in: *Introduction to Zeolite Science and Practice* (Eds: J. Cejka, H. van Bekkum, A. Corma, F. Schüth), Stud. Surf. Sci. Catal. 168, Chapter 8, Elsevier, Amsterdam **2007**.
[2] F. Kleitz, *Handbook of Heterogeneus Catalysis* (Eds: G. Ertl, H. Knoetzinger, F. Schueth, J. Weitkamp), Wiley-VCH Verlag GmbH & Co KgaA, Weinheim, **2008**.
[3] W. J. Roth, J. C. Vartuli, *Progress and Prospects, Studies in Surface Science and Catalysis* (Eds: J. Cejka, H. van Bekkum) 91, **2005**.
[4] T. J. Barton, M. Bull, W. G. Klemperer, D. A. Loy, B. McEnaney, M. Misono, P. A. Monson, G. Pez, G. W. Scherer, J. C. Vartuli, M. O. Yagi, *Chem. Mater.* **1999**, *11*, 2633.
[5] a) M. Hartmann., *Chem. Mater.* **2005**, *17*, 4577. b) M. Hartmann, D. Jung, *J. Mater. Chem.* **2010**, *20*, 844.
[6] J. Cejka, in: *Zeolites and Ordered Mesoporous Materials, Studies in Surface Science and Catalysis*, (Eds: J. Cejka, H. van Bekkum) 157, *111*, **2005**.
[7] S. Mintova, J. Cejka, in: *Introduction to Zeolite Science and Practice* (Eds: J. Cejka, H. van Bekkum, A. Corma, F. Schüth), Stud. Surf. Sci. Catal. 168, Chapter 15, Elsevier, Amsterdam **2007**, 495.
[8] F. Scheffler, W. Schwieger, D. Freude, H. Liu, W. Heyer, F. Janowski, *Microp. Mesop. Mater.* **2002**, *55*, 181.
[9] D. Serrano, J. Aguado, G. Morales, J. M. Rodriguez, A. Peral, M. Thommes, J. D. Epping, B. F. Chmelka, *Chemistry of Materials* **2009**, *21*, 641.
[10] W. Guo, L. Huang, P. Deng, Z. Xue, Q. Li, *Microp. Mesop. Mater.* **2001**, *44 – 45*, 427.
[11] O. Sel, D. Kuang, M. Thommes, B. Smarsly, *Langmuir* **2006**, *22*, 2311.
[12] a) B. G. Shpeizer, V. I. Bakhmutov, A. Clearfield, *Micropor. Mesopor. Mater.* **2006**, *90*, 81. b) B. G. Spheizer, V. I. Bakhmoutov, P. Zhang, A. Prosvirin, K. Dubar, M. Thommes, A. Clearfield, *Colloids and Surfaces A: Physicochem. Eng. Aspects* **2010**, *357*, 105.
[13] H. Li, M. Eddaoudi, M. O. Keefe, O. M. Yaghi, *Nature* **1999**, *402*, 276.
[14] G. Ferey *Introduction to Zeolite Science and Practice* (Eds: J. Cejka, H. van Bekkum, A. Corma, F. Schüth, Elsevier, Amsterdam **2007**.
[15] M. Hirscher, B. Panella, B. Schmitz, *Microp. Mesop. Mater.* **2010**, *129*, 335.
[16] J. Moellmer, E. B. Celer, R. Luebke, A. J. Cairns, R. Staudt, M. Eddaoudi, M. Thommes, *Micropor. Mesopor. Mater.* **2010**, *129*, 345.
[17] K. S. W. Sing, D. H. Everett, R. A. W. Haul, L. Mouscou, R. A Pierotti, J. Rouquerol, T. Siemieniewska, *Pure Appl. Chem.* **1985**, *57*, 603.
[18] S. J. Gregg, K. S. W. Sing, *Adsorption, Surface Area and Porosity*, Academic Press, London, **1982**.
[19] F. Rouquerol, J. Rouquerol, K. Sing, *Adsorption by Powders and Porous Solids*, Academic Press, London **1999**.
[20] S. Lowell, J. Shields, M. A. Thomas, M. Thommes, *Characterization of Porous Solids and Powders: Surface Area, Pore Size and Density*, Springer, The Netherlands, **2004**.
[21] A. Neimark, K. S. W. Sing, M. Thommes, *Surface Area and Porosity*, (Eds: G. Ertl, H. Koezinger, F. Schueth, J. Weitkamp), Wiley-VCH Verlag GmbH & Co KgaA, Weinheim, **2008**.
[22] M. Thommes, in: *Introduction to Zeolite Science and Practice* (Eds: J. Cejka, H. van Bekkum, A. Corma, F. Schüth), Stud. Surf. Sci. Catal. 168, Chapter 15, Elsevier, Amsterdam **2007**.
[23] M. Thommes, Physical Adsorption Characterization of Ordered and Amorphous Mesoporous Materials, in *Nanoporous Materials: Science and Engineering* (Eds: G. Q. Lu, X. S. Zhao), Imperial College Press, Oxford, 317, **2004**.

[24] J. C. Groen, L. A. Peffer, J. Perez-Ramirez, *Micropor. Mesopor. Mater.* **2003**, *60 (1 – 3)*, 1.
[25] a) R. Evans, U. M. B. Marconi, P. Tarazona, *J. Chem. Soc. Faraday Trans.* **1986**, *82*, 1763. b) P. Tarazona, U. M. B. Marconi, R. Evans, *Mol. Phys.* **1987**, *60*, 573.
[26] K. E. Gubbins, in *Physical Adsorption: Experiment, Theory and Application* (Eds: J. Fraissard), Kluwer, Dordrecht **1997**.
[27] a) A. V. Neimark, *Langmuir* **1995**, *11*, 4183. b) A. V. Neimark, P. I. Ravikovitch, M. Grün, F. Schüth, K. K. Unger, *J. Colloid. Interface Sci.* **1998**, *207*, 159. c) P. I. Ravikovitch, A. V. Neimark, *Langmuir* **2002**, *18*, 1550.
[28] J. P. Olivier, W. B. Conklin, V. Szombathley, *Stud. Surf. Sci. Catal.* **1994**, *87*, 81.
[29] L. D. Gelb, K. E. Gubbins, R. Radhakrishnan, M. Sliwinska-Bartkowiak, *Rep. Prog. Phys.* **1999**, *62*, 1573.
[30] A. V. Neimark, P. I. Ravikovitch, A. Vishnyakov, *Phys. Rev. E* **2000**, *62*, 1493.
[31] a) A. V. Neimark, P. I. Ravikovitch, *Microp. Mesop. Mater.* **2001**, *44*, 697. b) P. I. Ravikovitch, A. V. Neimark, *Col. Surf. A: Physicochemical and Engineering Aspects* **2001**, *187*, 11.
[32] M. Thommes, B. Smarsly, P. I. Ravikovitch, A. V. Neimark, *Langmuir* **2006**, *22*, 756.
[33] ISO-15901-3: Pore size distribution and porosity of solid materials by mercury porosimetry and gas adsorption – Analysis of micropores by gas adsorption, **2007**; ISO-15901-2: Pore size distribution and porosity of solid materials by mercury porosimetry and gas adsorption – Analysis of mesopores by gas adsorption, **2007**.
[34] Rouquerol, D. Avnir, C. W. Fairbridge, D. H. Everett, J. H. Haynes, N. Pernicone, J. D. F. Ramsay, K. S. W Sing, *Pure Appl. Chem.* **1994**, *66*, 1739.
[35] J. H Page, L. Liu, B. Abeles, E. Herbolzheimer, H. W. Deckmann, D. A. Weitz, *Phys. Rev. E* **1996**, *54*, 6557.
[36] B. Polarz, B. Smarsly, *J. Nanosc. Nanotechn.* **2002**, *6 (2)*, 581.
[37] E. Hoinkis, B. Roehl-Kuhn, *Langmuir* **2005**, *21*, 7366.
[38] L. A. Solovyov, O. V. Belousov, R. E. Dinnebier, A. N. Shmakov, S. D. Kirik, *J. Phys. Chem. B* **2005**, *109*, 3233.
[39] N. Muroyama, T. Ohsuna, R. Ryoo, Y. Kubota, O. Terasaki, *J. Chem. B* **2006**, *110*, 10630.
[40] A. I. Sagidullin, I. Furó, *Langmuir* **2008**, *24*, 4470.
[41] B. Smarsly, C. Göttner, M. Antonietti, W. Ruland, E. Hoinkis, *J. Phys. Chem. B* **2001**, *105 (4)*, 831.
[42] O. Sel, A. Brandt, D. Wallacher, M. Thommes, B. Smarsly, *Langmuir* **2007**, *23*, 4724.
[43] N. Muroyama, A. Yoshimura, Y. Kubota, K. Myasaka, T. Ohsuna, R. Ryoo, P. I. Ravikovitch, A. V. Neimark, M. Takata, O. Terasaki, *J. Phys. Chem C* **2008**, *112*, 10803.
[44] A. Zickler, S. Jähnert, W. Wagermaier, S. S. Funari, G. H. Findenegg, O. Paris, *Physical Review B* **2006**, *73*, 184109.
[45] S. Jähnert, D. Mueter, J. Prass, G. A. Zickler, O. Paris, G. H. Findenegg, *J. Phys.Chem.C* **2009**, *113*, 15201.
[46] S. Mascotto, D. Wallacher, A. Brandt, T. Hauss, M. Thommes, G. A. Zickler, S. S. Funari, A. Timmann, B. M. Smarsly , *Langmuir* **2009**, *25*, 12670.
[47] D. Vargas-Florencia, I. Furó, R. W. Corkery, *Langmuir* **2008**, *24*, 4827.
[48] J. U. Keller, R. Staudt, *Gas Adsorption Equilibria*, Springer, **2004**.
[49] R. S. H. Mikhail, Robens, *Microstructure and Thermal Analysis of Solid Surfaces*, Wiley, Chichester, **1983**.
[50] K. Kaneko, T. Ohba, Y. Hattori, M. Sunaga, H. Tanaka, H. Kanoh, *Stud. Surf. Sci. Catal.* **2002**, *144*, 11.
[51] J. Rouquerol, in *Physical Adsorption: Experiment, Theory and Applications* (Eds: J. Fraissard, C. W. Conner,) Kluwer, Dordrecht, 17, **1997**.
[52] W. C. Conner, in *Physical Adsorption: Experiment, Theory and Applications* (Eds: J. Fraissard, W. C. Conner), Kluwer, Dordrecht, 33, **1997**.
[53] J. Silvestre-Albero, A. Sepúlveda-Escribano, F. Rodríguez-Reinoso, V. Kouvelos, G. Pilatos, N. K. Kanellopoulos, M. Krutyeva, F. Grinberg, J. Kaerger, A. I. Spjeldavik, M. Stöcker, A. Ferreira, S. Brouwer, F. Kapteijn, J. Weitkamp, S. D. Sklari, V. T. Zaspalis, D. J. Jones, L. C. de Menorval, M. Lindheimer, P. Caffarelli, E. Borsella, A. A. G. Tomlinson, M. J. G. Linders, J. L. Tempelman, E. A. Bal, in: *Characterisation of Porous Solids VIII*, RSC, **2009**.
[54] J. Garcia-Martinez, D. Cazorla-Amoros, A. Linares-Solano, *Studies in Surface Science and Catalysis* **2000**, *128*, 485.
[55] S. T. Pauporté, J. Rathousky, *J. Phys. Chem. C* **2007**, *111*, 7639.
[56] M. Thommes, S. Tanaka, N. Nishyama, *Stud. Surf. Sci. Catal.* **2007**, *165*, 551.
[57] F. Hung, K. E Bhattacharya, B. Coasne, M. Thommes, *Adsorption* **2007**, *13*, 425.
[58] M. Thommes, R. Koehn, M. Froeba, *Appl. Surf. Sci.* **2002**, *196 (1 – 4)*, 239.
[59] M. Thommes, R. Köhn, M. Fröba, *J. Phys. Chem. B* **2000**, *104*, 79.
[60] M. W. Cole, W. F. Saam, *Phys. Rev. Lett* **1974**, *32*, 985.
[61] J. Frenkel, *Kinetic Theory of Liquids*, Oxford University Press, **1946**.
[62] G. D. Halsey, *J. Chem. Phys.* **1948**, *16*, 931.
[63] T. L. Hill, *Advances in Catalysis IV*, Academic Press, N.Y., 236, **1952**.
[64] a) W. T. Thompson, *Philos. Mag.* **1871**, *42*, 448. b) Z. Zsigmondy, *Anorg. Chem.* **1911**, *71*, 356.
[65] a) L. H. J. Cohan, *J. Am. Chem. Soc.* **1938**, *60*, 433. b) L. H. Cohan, *J. Am. Chem. Soc.* **1944**, *66*, 98.
[66] E. P. Barrett, L. G. Joyner, P. P. Halenda, *J. Am. Chem. Soc.* **1951**, *73*, 373.
[67] D. H Everett, in: *The Solid-Gas Interface*, (Ed: E. A. Flood), Marcel Decker, N.Y., 2, **1967**.
[68] P. A. Monson, *Langmuir* **2008**, *24*, 12295.

[69] a) P. C. Ball, R. Evans, *Langmuir* **1989**, *5*, 714. b) R. J. Evans, *Phys. Condens. Matter.* **1990**, *2*, 8989.
[70] P. I. Ravikovitch, A. V. Neimark, *Langmuir* **2000**, *16*, 2419.
[71] R. Valiullin, S. Naumov, P. Galvosas, J. Kaerger, H.-J. Woo, F. Porcheron, P. A. Monson, *Nature* **2006**, *443*, 965.
[72] M. Thommes, R. Koehn, M. Froeba, *Stud. Surf. Sci. Catal.* **2002**, *142*, 1695.
[73] F. Kleitz, F. Berube, C.-M. Yang, M. Thommes, *Stud. Surf. Sci. Catal.* **2007**, *170*, 1843.
[74] R. Nicolas, F. Berube, T. W. Kim, M. Thommes, F. Kleitz, *Stud. Surf. Sci. Catal* **2008**, *174*, A 141.
[75] F . Kleitz, F. Berube, R. Guillet-Nicolas, C.-M. Yang, M. Thommes, *J. Phys. Chem. C* **2010**, in press.
[76] M. Morishige, K. Tateishi, S. Fukuma, *J. Phys. Chem B.* **2003**, *107*, 5177.
[77] B. Coasne, A. Galarneau, F. Di Renzo, R. M. Pellenq, *Langmuir* **2006**, *22*, 11097.
[78] A. V. Neimark In *Characterization of Porous Solids III* (Eds: J. Rouquerol, F. Rodriguez-Reinoso, K. S. W. Sing, K. K. Unger), *Studies in Surface Science and Catalysis 87*, Elsevier, Amsterdam **1994**, 67.
[79] V. Magyota, F. Rojas, I. Kornhauser, *J. Chem. Soc. Faraday Trans I* **1985**, *81*, 2931.
[80] F. Casanova, C. E. Chiang, C. P. Li, I. K. Schuller, *Applied Phys. Lett.* **2007**, *91*, 243103.
[81] J. H. De Boer, *The Structure and Properties of Porous Materials*, Butterworths, London, **1958**.
[82] E. O. Kraemer, in *Treatise on Physical Chemistry*, D. van Nostrand, N.Y. **1931**.
[83] J. W. J. McBain, *J. Am. Chem. Soc.* **1935**, *57*, 699.
[84] G. Mason, *J. Coll. Interf. Sci.* **1982**, *88*, 36.
[85] a) A. V. Neimark, *Rep. Acad. Sci., USSR (Phys. Chem.)* **1983**, *273*, 867. b) A. V. Neimark, *Colloid J., USSR* **1986**, *46*, 1004.
[86] a) L. Z. Zhang, N. A. Seaton, *Langmuir* **1993**, *9*, 2576. b) H. Liu, N. A. Seaton, *Chem. Eng. Sci.* **1994**, *49*, 1869.
[87] F. Rojas, I. Kornhauser, C. Felipe, J. M. Esparza, S. Cordero, A. Dominguez, J. L. Riccardo, *Phys. Chem. Phys.* **2002**, *4*, 2346.
[88] A. V. Neimark, *Stud. Surf. Sci. Catal.* **1991**, *62*, 67.
[89] M. Parlar, Y. C. Yortsos, *J. Coll. Interf. Sci.* **1988**, *124*, 162.
[90] H. Zhu, L. Zhang, N. A. Seaton, *Langmuir* **1993**, *9*, 2576.
[91] M. Kruk, E. B. Celer, J. Matos, S. Pikus, M. Jaroniec, *J. Phys. Chem. B* **2005**, *109*, 3838.
[92] K. Morishige, M. Tateishi, F. Hirose, K. Aramaki, *Langmuir* **2006**, *22*, 9220.
[93] H. J. Woo, L. Sarkisov, P. A. Monson, *Langmuir* **2001**, *17*, 7472.
[94] L. Sarkisov, P. A. Monson, *Langmuir* **2001**, *17*, 7600.
[95] a) P. I. Ravikovitch, A. V. Neimark, *Langmuir* **2002**, *18*, 1550. b) P. I. Ravikovitch, V. Neimark, *Langmuir* **2002**, *18*, 9830.
[96] A. Vishnyakov, A. V. Neimark, *Langmuir* **2003**, *19*, 3240.
[97] B. Libby, V. Monson, *Langmuir* **2004**, *20*, 6482.
[98] B. Smarsly, M. Thommes, P. I. Ravikovitch, A. V. Neimark, *Adsorption* **2005**, *11*, 653.
[99] T. W. Kim, R. Ryoo, M. Kruk, K. P. Gierszal, M. Jaroniec, S. Kamyia, O. Terasaki, *J. Phys. Chem. B* **2004**, *108*, 11480.
[100] C. Bisio, G. Gatti, E. Boccaleri, L. Marchese, L. Bertinetti, S. Coluccia, *Langmuir* **2008**, *24*, 2808.
[101] C. J. Rasmussen, A. Vishnyakov, M. Thommes, B. M. Smarsly, F. Kleitz, A. V., Neimark, *Langmuir* **2010**. DOI: 10.1021/la100268q
[102] P. van der Voort, P. I. Ravikovitch, K. P. De Jong, A. V. Neimark, A. H. Janssen, M. Benjelloun, E. van Bavel, P. Cool, B. M. Weckhuysen, E. F. Vansant, *Chem. Commun.* **2002**, 1010.
[103] S.-E. Park, N. Jiang, in *Zeolites: From Model Materials to Industrial Catalysis* (Eds: J. Cejka, J. Perez-Pariente, W. J. Roth, Eds), 81, **2008**.
[104] a) O. Kadlec, M. M. J. Dubinin, *Coll. Interf. Sci.* **1969**, *31*, 479. b) C. G. V. Burgess, D. H. Everett, *J. Coll. Interf. Sci.* **1970**, *33*, 611.
[105] A. Schreiber, S. Reinhardt, G. H. Findenegg, *Stud. Surf. Sci. Catal.* **2002**, *144*, 177.
[106] C. G. Sonwane, S. K. Bhatia, *Langmuir* **1999**, *15*, 5347.
[107] S. Brunauer, P. H. Emmett, E. Teller, *J. Amer. Chem. Soc.* **1938**, *60*, 309.
[108] F. Rouquerol, J. Rouquerol, C. Peres, Y. Grillet, M. Boudellal, in: *Characterization of Porous Solids* (Eds: S. J. Gregg, K. S. W. Sing, H. F. Stoeckli), The Society of Chemical Industry, 107, **1978**.
[109] J. Rouquerol, P. Llewellyn, F. Rouquerol, *Stud. Surf. Sci. Catal.* **2007**, *160*, 49.
[110] K. S. Walton, R. Snurr, *J. Am. Chem. Soc.* **2007**, *129*, 8552.
[111] A. Galarneau, D. Desplantier, R. Dutartre, F. Di Renzo, *Microp. Mesop. Mater.* **1999**, *27*, 107.
[112] L. Jelinek, E. S. Kovats, *Langmuir* **1994**, *10*, 4225.
[113] ISO-FDIS 9277:2010.
[114] M. M. Dubinin, L. V. Radushkevitch, *Dokl. Akad. Nauk, S.S.S.R.* **1947**, *55*, 331.
[115] G. Horvath, K. Kawazoe, *J. Chem. Eng. Japan* **1983**, *16*, 47.
[116] a) A. Saito, H. C. Foley, *Am. Inst. Chem. Eng.* **1991**, *37*, 429. b) A. Saito, H. C. Foley, *Microp. Mesop. Mate.* **1995**, *3*, 531.
[117] M. Kruk, M. Jaroniec, A. Sayari, *J. Phys. Chem. B* **1997**, *101*, 583.
[118] M. Jaroniec, A. L. Solovyov, *Langmuir* **2006**, *22*, 6757.
[119] F. Kleitz, T. Czuryszkiewics, L. A. Solovyov, M. Linden, *Chem. Mater.* **2006**, *18*, 5070.
[120] A. Zukal, M. Thommes, J. Cejka, *Microporous Mesoporous Mater.* **2007**, *104*, 52.
[121] E. A. Ustinov, D. D. Do, V. B. Fenelonov, *Carbon* **2006**, *44*, 653.
[122] P. Ravikovitch, A. V. Neimark, *Langmuir* **2006**, *160*, 11171.
[123] A. V. Neimark, Y. Li, P. I. Ravikovitch, M. Thommes, *Carbon* **2009**, *47 (7)*, 1617.
[124] J. Jagiello, J. P. Oliver, *J. Phys. Chem. C* **2009**, *113 (45)*, 19382.

